4

High-Field, Pulsed, and Double Resonance Studies of Crude Oils and their Derivatives

Marat Gafurov[1], M. Volodin[1,2], T. Biktagirov[1], G. Mamin[1] and S. B. Orlinskii[1]*

[1] *Kazan Federal University, Kremlevskaya, 18, Kazan, 420008, Russia*
[2] *Sakhalin Energy Investment Company, Ltd., Dzerzhinskogo, 35, Yuzhno-Sakhalinsk, 693020, Russia*

4.1 Introduction

A typical petroleum fluid can be considered as a petroleum disperse system (PDS): a hybrid of a solution and a colloidal dispersion (of crystallizing waxes, self-associating asphaltenes, etc.) (Syunyaev, 1980). Understanding the complex behavior of PDS is a challenge. Nevertheless, as stressed by Evdokimov, Eliseev, and Eliseev (2001, 2004), relatively simple experiments on only one of the PDS components can shed light on details of the structural features and transformations in such systems.

As one of the constituents of PDS, a paramagnetic phase can be the subject of interest: one gram of PDS contains 10^{16}–10^{21} paramagnetic centers (PCs) (Yen and Chilingarian, 1994, 2000). The majority of PC is concentrated in the high-molecular PDS components, such as asphaltenes, resins, and polycyclic aromatic hydrocarbons. The content of the high-molecular PDS components could reach the values of 45 wt% in native oils and up to 73 wt% in natural asphalts and bitumen. Assuming that asphaltenes and resins have a molecular weight of about 1000 Da (Yen and Chilingarian, 1994), they could contain up to one unpaired electron per molecule. Obviously, such a high concentration of PC should affect not only the paramagnetic properties of substance but (at least partially) also the other ones (the electrical qualities of PDS, for example). The analysis of the behavior of the intrinsic PC in PDS could complement the data obtained by other established analytical tools.

Figure 4.1 gives a brief look into the nature of some PCs in condensed matter. The existence of intrinsic PC in PDS is caused mainly by the presence of *d*-metals (first of all V, Ni, Fe) and stable "free" radicals (FR) in PDS. It is usually

*Corresponding author: volodinmikhail@yandex.ru

Analytical Characterization Methods for Crude Oil and Related Products, First Edition.
Edited by Ashutosh K. Shukla.

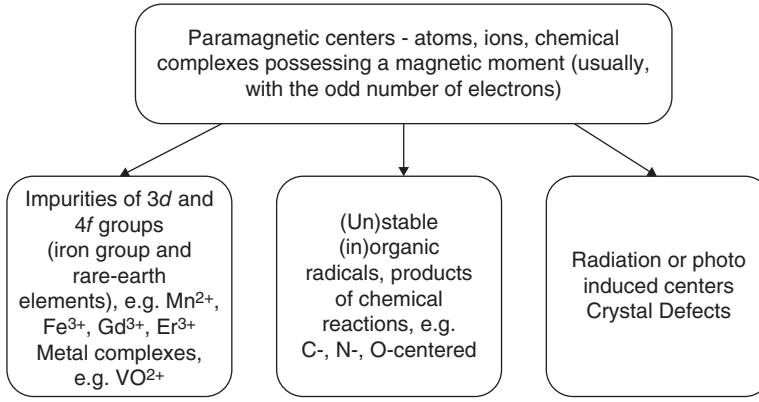

Figure 4.1 Types of paramagnetic centers.

assumed that FR in PDS are mainly concentrated in asphaltenes and arise due to the delocalized π-electrons of the aromatic rings and stable organic radicals of the side chains (Yen and Chilingarian, 1994, 2000). Here we have to note that the exact location and structure of FR in PDS are still undefined and the researchers are conventionally referred to the PC detected in coals (Yen and Chilingarian, 2000).

One of the most powerful methods to detect PCs, identify them, derive their concentrations, establish the structure of the paramagnetic complexes, etc. is the group of techniques of electron paramagnetic resonance (EPR) also named electron spin resonance (ESR). Figure 4.2 presents different modern

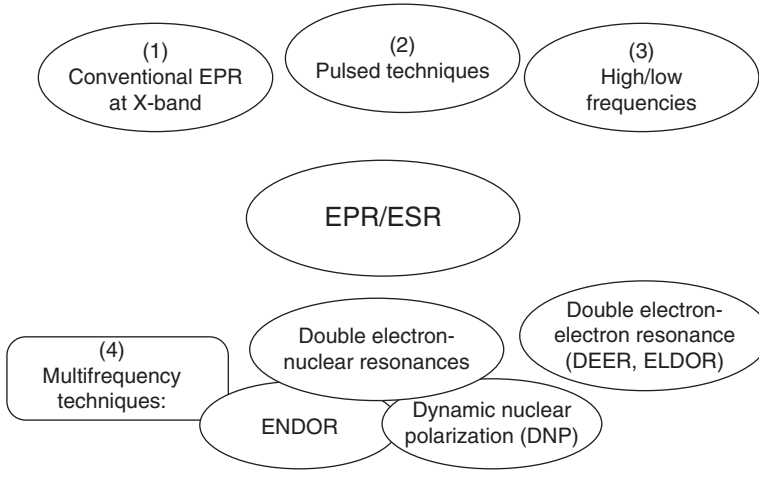

Figure 4.2 The variety of the modern commercially realized EPR techniques.
Source: Stoll and Schweiger (2006). Reproduced with permission of Elsevier.

commercially realized EPR techniques for material analysis that are also widely applied in biochemical/biomedical research (Qin and Warncke, 2015a, 2015b; Burlaka *et al.*, 2016). The reader will be acquainted with the most of them on particular examples in this manuscript. Surprisingly, the abilities of the modern EPR techniques are practically not known in oil-related research (at least so far as we can judge based on the analysis of the open sources). The overwhelming majority of EPR studies are still based on the application of routines of the conventional EPR at X-band with the microwave frequency of approximately 9 GHz (Piccinato, Guedes, and Di Mauro, 2012; Trukhan *et al.*, 2014; Wang *et al.*, 2016; Dolomatov *et al.*, 2016) that were established between the 1950s and 1970s (see Yen and Chilingarian, 1994; Garifyanov and Kozyrev, 1956; Gutowsky *et al.*, 1958; O'Reilly, 1958).

The last few years have seen an increased interest in studying unfractionated PDS by pulsed and high-frequency EPR (Ramachandran *et al.*, 2015; Tayeb Ben *et al.*, 2015; Mamin *et al.*, 2016; Gracheva *et al.*, 2016). One of the aims of this chapter is to show some applications of the "unconventional" EPR techniques and to encourage oil-related specialists to use different EPR approaches. This family of techniques does not face the problem of extraction and dilution of samples (in contrast to optical analysis, for example) and gives us the opportunity to probe the native structure and dynamical properties of PDS. Besides the higher sensitivity and spectral resolution, the advantages of the high-field EPR approaches for the identification of different paramagnetic complexes and their characterization in native oil containing formations are discussed here. For instance, in case of even slight anisotropy of magnetic interaction tensors (such as g and hyperfine tensors), high-field EPR approaches can provide the information about their orientation dependencies and thereby about the spatial structure of the paramagnetic complexes in disordered systems.

This work represents our particular vision based on our experience gathered so far, and does not pretend to be complete. This chapter presents only those experiments and data that were obtained at the Institute of Physics of Kazan Federal University in collaboration with other departments of Kazan Federal University and A. E. Arbuzov Institute of Organic and Physical Chemistry of Russian Academy of Sciences, Kazan, Russia.

4.2 EPR: Basic Principles and Magnetic Interactions

EPR is an effect of the resonant absorption of electromagnetic radiation by unpaired electrons placed in a constant magnetic field. Absorption starts when the frequency of an electromagnetic field coincides with the frequency of an electron's magnetic moment precession. Figure 4.3 demonstrates the reconstruction of the original experimental setup with which the EPR phenomenon was discovered by Evgeny K. Zavoisky in Kazan State University in 1944 (Zavoisky, 1945).

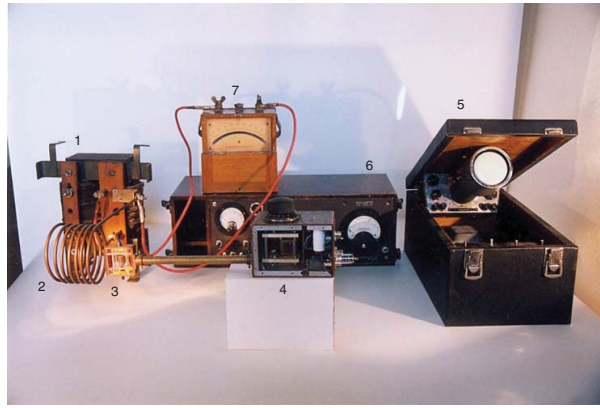

Figure 4.3 Reconstruction of the first EPR machine of E. K. Zavoisky operating at 10 MHz on which the first EPR spectrum in the world was observed in 1944. Courtesy of Igor Silkin, the keeper of E. K. Zavoisky Museum at Kazan Federal University. (1) Transformer. (2) Solenoid supplied by transformer and producing a low-frequency magnetic field that substituted constant magnetic field in this setup. (3) Ampoule with sample inserted into resonator–radio frequency coil, oriented perpendicular to solenoid axis. (4) Autodyne generator working at 10 MHz and signal preamplifier. (5) Oscilloscope. (6) A rheostat for adjusting the current through the transformer. (7) Ammeter used to control the magnetic field inside the solenoid, which is proportional to the alternating current value at the transformer's secondary coil.

Table 4.1 EPR microwave frequency bands with the corresponding wavelengths, energies, and typical magnetic fields for $g = 2$.

Band	Typical frequency, GHz	Wavelength, mm	Energy, cm^{-1}	Magnetic field at $g = 2$, T
L-band	1	300	0.03	0.03
S-band	3	100	0.1	0.11
X-band	9	33	0.3	0.32
Q-band	35	8, 5	1.2	1.25
W-band	95	3	3.2	3.4
G- (or J-) band	263	1	9.5	10.2

Today, the X-band machines (operating at the microwave frequency of ν = 9–10 GHz) are exploited routinely, though apparatus for other frequencies are available (see Table 4.1). Bruker Corporation holds the greatest global share of the production of EPR spectrometers (Bruker, 2016). However, for routine analysis and specific applications a lot of the producers can be found on the market: Adani, Freiberg Instruments (Magnettech), Yaviar, etc. (Adanisystems, 2016; Magnettech, 2016, Yaviar, 2016). The data presented in this manuscript have been obtained using Bruker ELEXSYS 680 (W-band, $\nu = 94$ GHz), Bruker ESP-300 and LABRADOR (both the X-band) EPR spectrometers. Figure 4.4

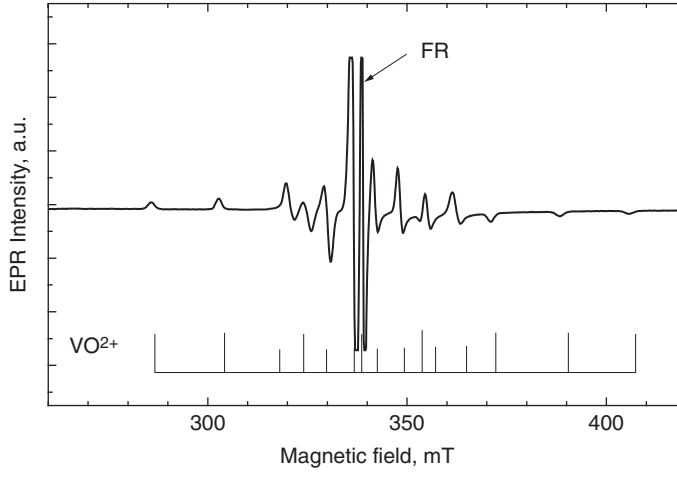

Figure 4.4 Typical EPR spectrum of crude oil sample at X-band at near room temperature.

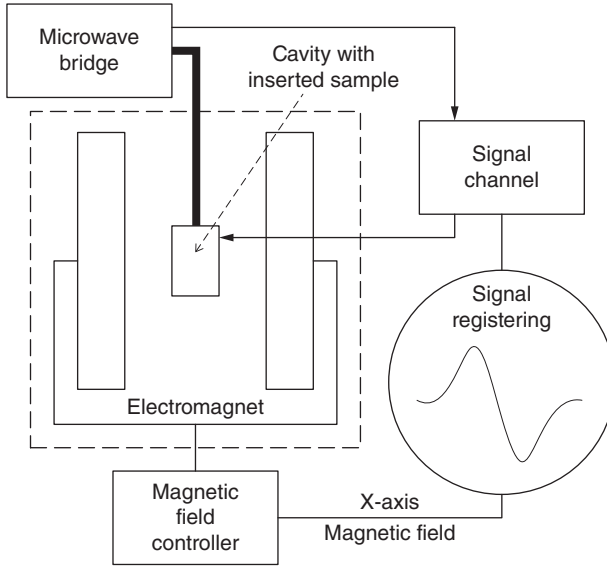

Figure 4.5 The simplified scheme of the conventional EPR spectrometer.

presents typical conventional EPR spectra of crude oil at room temperature (RT). As already mentioned, it is due to FR mainly localized within the polyaromatic condensed nuclei of the asphaltene molecules and VO^{2+} complexes and is discussed in detail below. Usually, the position/lineshape/intensity of the FR and VO^{2+} and the intensity ratio between the FR and vanadyl signals, which serve as the fingerprint of the hydrocarbon origin, are analyzed.

The core elements of the construction of the conventional EPR spectrometers are still the same as for Zavoisky's machine (see Figure 4.5). Typically, the PDS samples are placed in the quartz or glass tubes and then into the EPR cavity (see Figure 4.6). The simple microwave cavity is a metal box with a rectangular or cylindrical shape which resonates with microwaves. Cavity has the geometrical size of about the corresponding wavelength (see Table 4.1). The cavity is an analogue of LC circuit in nuclear magnetic resonance (NMR) and serves to store the microwave energy and to separate the electrical and magnetic components of electromagnetic field because the magnetic one causes the EPR transitions while the electrical component can cause an undesirable sample heating (Eaton *et al.*, 2010). As is shown in Figure 4.6, high-field machines require much less sample volume (of about 500 nL for W-band) that can be an advantage when the limited in amount species should be examined by different analytical methods, after different treatments, etc.

EPR often uses a technique known as phase sensitive detection to enhance the sensitivity of the spectrometer. In this approach the magnetic field

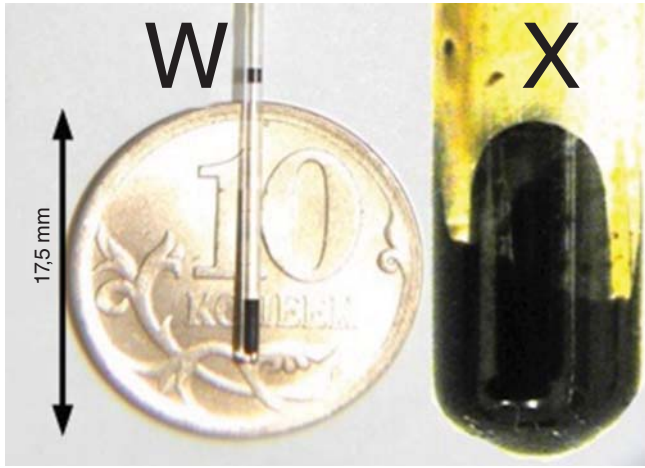

Figure 4.6 Commonly used EPR tubes for PDS samples in the W-band and X-band EPR spectrometers.

strength is modulated by sinusoidal signal with the amplitude of 0.1–1 mT and modulation frequency of about 10–100 kHz. It leads (as a rule) to the record of the first derivative curve of the EPR absorption signal, as shown in Figure 4.4, for example. Therefore, the concentration of the PC can be derived after the double integration of the recorded spectrum. The advantages are that it encodes the EPR signals to make it distinguishable from sources of noise or interference and provides the elimination of baseline instabilities due to the drift in DC electronics (Eaton *et al.*, 2010). In the pulsed mode (see Section 4.3), one can obtain a spectrum that is very often named field-swept electron spin echo (FS-ESE), which is usually close to the absorption spectrum. In some cases (for low-viscous crude oils, for example) low temperatures ($T < 250$ K) are necessary to slow down the electronic relaxation times to be able to obtain spin-echo or FS-ESE with the perceptible signal-to-noise ratio.

Both conventional and FS-ESE EPR spectra are sensitive to a number of interactions between the unpaired spin and the environment:

- the Zeeman interaction between the unpaired spin and the external magnetic field;
- the spin orbit coupling;
- the electron spin–nuclear spin interactions;
- the interaction with other unpaired electrons (spin–spin interaction).

The largest interaction in most cases (especially at W-band frequencies, see Table 4.1) and the one which EPR is based on is the Zeeman effect (see Figure 4.7). The essential aspects of EPR may be illustrated by considering the

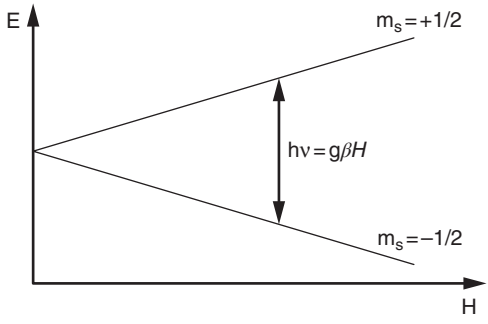

Figure 4.7 The Zeeman effect. An increasing magnetic field is applied in the presence of a fixed microwave frequency. When the resonance condition is reached (position of the arrow), an absorption occurs between the lower energy level (spin magnetic quantum number $m_s = -1/2$) and the upper energy level ($m_s = +1/2$). The energy difference is quantized and is equivalent to the term $g\beta H$.

hypothetical case of a single isolated electron. This electron is characterized by the quantum number $S = 1/2$ and possesses a magnetic moment

$$\overline{\mu}_s = g\beta\overline{S}, \tag{4.1}$$

where $g = 2.0023$ is the electron g-factor (that is sensitive to the spin–orbit interaction, chemical neighborhood of the unpaired electron and, consequently, to structure properties of sample material), $\beta = 9.274 \cdot 10^{-24}$ J·T^{-1}, the electronic Bohr magneton, and $\overline{S}$, the dimensionless electron spin vector. In a magnetic field, there are two energy states for this electron, as illustrated in Figure 4.7. Typical g-factors for PC in PDS are in the range of 1.96 (for VO^{2+}) up to 2.008 (sulfur-containing radicals), which implies the application of magnetic fields B of 0.35 T for X-band and of 3.5 T for W-band to match resonance condition. It implicates a use of superconducting magnets for high microwave frequencies.

Another interaction (commonly applicable to hydrocarbon systems) is the spin–nuclear one. As a nucleus could also have a magnetic moment, the interaction of the unpaired electron with the nucleus splits the electron energy levels, generating a structure called a hyperfine (hf) structure in the EPR spectrum. Each "m_s level" splits into a closely spaced group of $(2I + 1)$ levels, where I is the nuclear spin quantum number.

Only transitions are allowed with $\Delta m_S = \pm 1$ and $\Delta m_I = 0$. Each one of these transitions gives rise to a resonance line in the EPR spectrum. The spacing between the observed lines is the hf coupling constant (A). An analysis of hf splitting of EPR spectra among others again allows us to investigate the structure of the electron's neighborhood. Atoms in the vanadyl porphyrins ($^{51}V^{4+}$, $3d^1$, electronic spin $S = 1/2$, nuclear spin $I = 7/2$) are arranged practically in a plane defining thus the anisotropic g-factor and hf A tensor of axial symmetry (see Figure 4.8). The powder EPR spectrum of the vanadyl ions consists of the 16 "lines" representing the 2×8 hf patterns (the projection of I is allowed to take eight values: $\pm 7/2$; $\pm 5/2$; $\pm 3/2$; $\pm 1/2$) for the parallel and the perpendicular complex orientations (see Figure 4.4 and Figure 4.9).

Petroleum porphyrins in PDS exist in homologous manifolds of several structural classes that contain different types of substitutions and binding moieties. These determine the range of EPR parameters (especially $A_{\perp}$ and $A_{||}$) not only for different PDS samples but even within each of them.

4.3 EPR Pulse Sequences

Pulse methods are able to significantly increase and supplement information obtained from conventional EPR spectra (Schweiger and Jeschke, 2001). While stationary methods use continuous microwave irradiation and reveal splitting of energy levels of paramagnetic system, pulse techniques provide insights into the dynamics of the system and allows us to measure relaxation times, decode complex EPR spectra of several interacting PC, etc.

The main feature of the pulse EPR spectrometer is the presence of an additional pulse former device consequently connected with the microwave generator. As for most NMR spectrometers, the pulses could be applied using several channels. They can be combined into special sequences with the ability to change pulse duration and delays between them. But because the electronic relaxation times (longitudinal or spin-lattice relaxation time T_{1e} and transverse or spin-spin relaxation time T_{2e}) are of 3–6 orders of magnitude shorter than

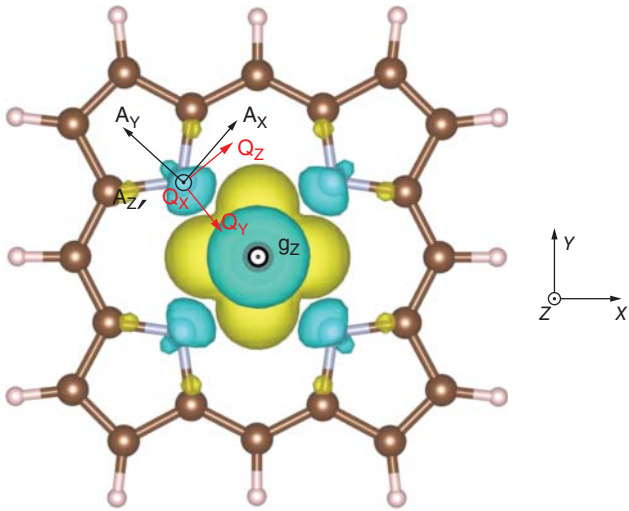

Figure 4.8 Schematic representation of a vanadyl porphyrin molecule backbone. The orientations of nitrogen hf (*A*) and quadrupole coupling (*Q*) tensors derived from DFT calculations are shown for a selected nuclei. Spatial distribution of spin density is visualized as an isosurface. X–Y–Z axes of the molecular frame are shown with the Z axis perpendicular to the porphyrin plane. As shown, the calculated g_z is collinear with the molecular Z axis.

the nuclear ones, the characteristic time parameters are also much shorter. The typical pulse sequences we use in our PDS-related research in the W-band are: (1) $\pi/2{-}\tau{-}\pi$ with the $\pi/2$ pulse duration of 32 ns and the time delay $\tau = 240$ ns to obtain electron spin echo (ESE); (2) T_{2e} is studied by tracking the primary ESE amplitude with the same $\pi/2{-}\pi$ pulse durations while varying τ with the minimal possible step of 4 ns; (3) T_{1e} is extracted from an inversion-recovery studies by applying the $\pi{-}T_{\text{delay}}{-}\ \pi/2{-}\tau{-}\ \pi$ pulse sequence, where π pulse

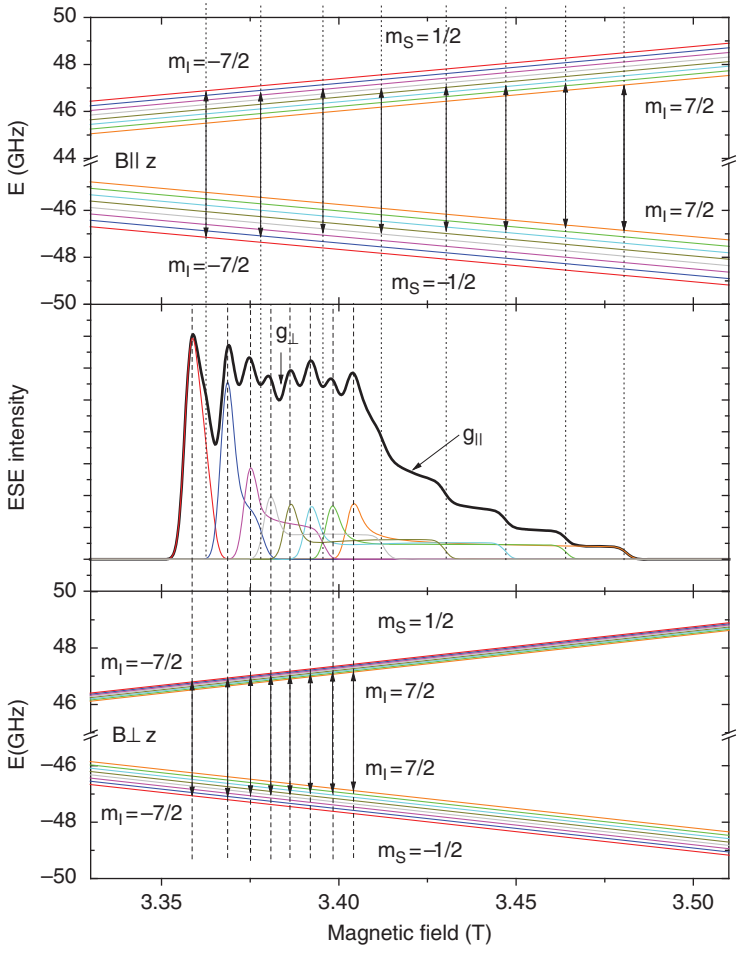

Figure 4.9 The energy levels and the corresponding absorption EPR spectrum for VO^{2+} complex calculated for the microwave frequency $\nu = 94$ GHz, $g_{||} = 1.963$, $g_{\perp} = 1.985$, $A_{||} = 470$ MHz, $A_{\perp} = 150$ MHz. Particular contributions from every EPR transition are color marked. Calculations are done in EasySpin package for Matlab (Stoll and Schweiger, 2006).

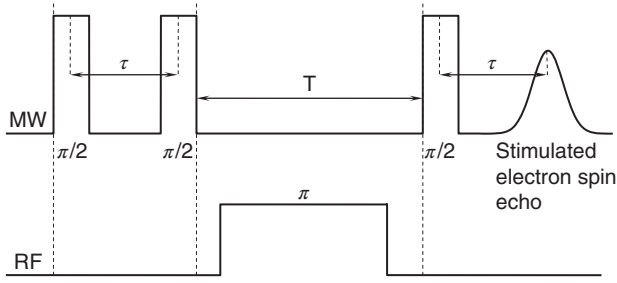

Figure 4.10 Mims pulse sequence at microwave and radio frequencies used to obtain the ENDOR spectra as a function of stimulated electron spin echo amplitude from the frequency of RF pulse.

duration and τ are fixed (64 ns and 240 ns, correspondingly) while T_{delay} is varied.

For electron nuclear double resonance (ENDOR) experiments we used special double (for nuclei and electron) cavities and Mims pulse sequence $\pi/2{-}\tau{-}\pi/2{-}T{-}\pi/2$ with an additional radio frequency (RF) pulse $\pi_{\text{RF}} = 16$ μs inserted between the second and third microwave $\pi/2$ pulses (see Figure 4.10). RF frequency in our setup could be swept in the range of 1–200 MHz.

Some ENDOR basics are briefly described below. One can find more details in the referenced works (Murphy and Farley, 2006; Yavkin *et al.*, 2014).

In the case of a "free" nucleus, RF pulse applied at the Larmor frequency

$$\nu_{Larmor} = |\gamma B_0| \equiv h^{-1}|g_I \beta_I B_0|, \tag{4.2}$$

where γ is a gyromagnetic ratio of the nuclear spin I, h is a Planck constant, g_I is a nuclear g-factor and β_I is a nuclear Bohr magneton, it can change the state of the nuclear spin (the population of the nuclear sublevels). For ^{1}H with $\gamma_{1\text{H}} =$ 42.576 MHz/T that results in $\nu_{Larmor} \approx 144.76$ MHz for $B_0 = 3.4$ T.

In the case of the coupled electron spin S such changing of the nuclear spin can modify the state of the electron spin (can change the population of the energy levels contributing to the EPR spectrum). For the hf coupling constant A and simple electron–nuclear coupling ($S = 1/2$, $I = 1/2$), it can lead to the appearance of the characteristic features in the ENDOR spectrum at the radio frequencies

$$\nu_{ENDOR} = \nu_{Larmor} \pm A/2 \quad \text{or} \tag{4.3}$$

$$\nu_{ENDOR} = A/2 \pm \nu_{Larmor}, \tag{4.4}$$

depending on the ratio between A and ν_{Larmor}.

The ENDOR splitting a_{ENDOR} can help not only to identify a type of nuclei coupled with the electron spins but also to provide spatial relationships between them. For the pure electron–nuclei dipole–dipole interaction in the

point model, the electron–nuclear distance r from the ENDOR splitting can be estimated from

$$a_{ENDOR} \approx g \cdot g_I \cdot (1 - 3\cos^2\theta)/r^3, \tag{4.5}$$

where g is a g-factor of electron spin S, Θ is an angle between directions of the parallel component of g ($g_{||}$) and B_0. As it follows from Equation 4.5, a_{ENDOR} depends on the distance between the electron and nuclear spins and their mutual orientation. In this work we consider ENDOR splitting due to the interaction of vanadyl electron spin and ^{1}H nuclear spins with $S = I = 1/2$ and with ^{14}N nuclear spins with $I = 1$. The values of B_0 at which the ENDOR spectra were measured were defined by the particular values of angle Θ (see Section 4.4).

Additionally, for $I = 1$ an electric nuclear quadrupole coupling exists that can split or shift the ENDOR lines: the nuclear quadrupole interaction is sensitive to the electric field gradient at the site of the nucleus.

4.4 Application Examples

4.4.1 W-Band, Relaxation Studies of VO^{2+} and FR in Asphaltenes Fractions

We have investigated 12 asphaltenes powders that were precipitated from the raw material of different oxidized bitumen and heavy crude oils from the oil refineries and oilfields of the Republic of Tatarstan (Russia) and Kazakhstan by the addition of the petroleum ether (bp 40–70 °C) using a Soxhlet apparatus. Then the filtered asphaltenes were washed out with the benzene, which was then evaporated. The obtained fraction is called A_{init}.

The *A1* and *A2* fractions of asphaltenes were obtained as follows (see Figure 4.11). One gram of A_{init} asphaltenes was first completely dissolved with

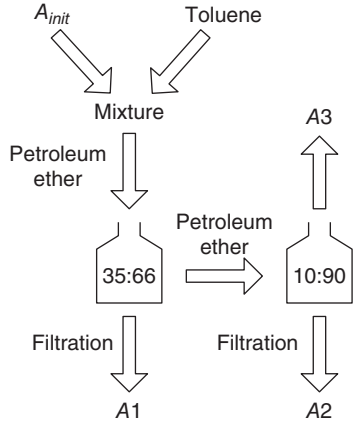

Figure 4.11 The scheme of fractionation of asphaltenes.

28 mL toluene. Petroleum ether (bp 40–70 °C) was then added in the amount of 52 mL. The resulting solution was kept in a dark place for 24 h and then filtered. Precipitated material was washed in a Soxhlet apparatus with toluene until the solvent became colorless, dried, and weighed until there was no change in its mass. The obtained fraction was called *A1*.

Then the petroleum ether was added to the supernatant in the amount of 228 mL and precipitated for 24 h. Using the operations described above, the fresh precipitated material was separated, washed with toluene in a Soxhlet apparatus, and dried. *A2* fraction of asphaltenes was recovered by evaporating the remaining solvent. The investigated samples are listed in Table 4.2.

Figure 4.12 demonstrates a typical FS-ESE detected EPR spectrum at T = 40 K and repetition time of 0.5 μs to intensify the VO^{2+} component of the spectrum. Small difference in the values of g-factors for FR and VO^{2+} allows them to be resolved spectrally and their relaxation times measured separately. The relaxation times were measured at the magnetic fields corresponding to the maximum of ESE signal (marked in Figure 4.12).

The relaxation constants in the T_{1e} processes of the longitudinal relaxation defined under an assumption of its monoexponential character for all the studied samples are presented in Figure 4.13. It can be seen that $T_{1\mathrm{FR}}$ is much longer than $T_{1\mathrm{VO}}$ and, in contrast to the vanadyl complexes, changes significantly from sample to sample and from fraction to fraction. Taking into account that the molecules forming the asphaltenes in both fractions *A1* and *A2* are of comparable size, the difference in the relaxation rates reflects the fact that the FR surrounding in fractions *A1* and *A2* is different while the same fractions' treatment does not change surrounding VO^{2+}. We suppose, therefore, that $T_{1\mathrm{FR}}$ and $T_{1\mathrm{VO}}$ measurements could be used to track the processes of polymerization, chemical or thermal treatments of PDS, etc., in which a role (as yet perhaps undefined, or even multiple roles) for PC is expected. Additional experimental and theoretical efforts are needed to increase our understanding of the main mechanisms defining the longitudinal relaxation in asphaltenes.

Transverse relaxation times of the vanadyl complexes in asphaltenes are also significantly shorter than those for FR, and in all the samples a single

Table 4.2 List of the studied samples.

Sample	Raw Material	Source	Investigated fractions of asphaltenes
# 1	Oxidized bitumen	Oil refinery #1	
# 2	Oxidized bitumen	Oil refinery #2	A_{init}, *A1*, *A2*
# 3	Crude oil	Russian oilfield	
# 4	Crude oil	Kazakhstan oilfield	

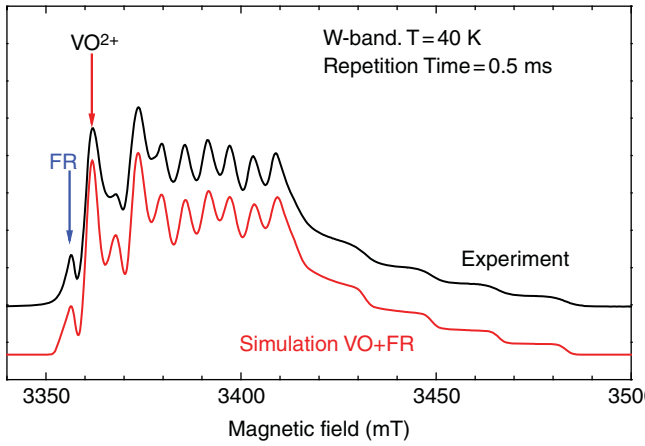

Figure 4.12 Typical W-band EPR spectrum of asphaltene fraction *A1* for sample #3 in pulsed mode at $T = 40$ K and repetition time of 0.5 μs along with its simulation as a sum of VO^{2+} powder spectra with $g_{||} = 1.964$, $g_{\perp} = 1.984$, $A_{||} = 16.8$ mT, $A_{\perp} = 6.0$ mT, and FR single line with $g = 2.0036$. Arrows FR and VO^{2+} mark the values of B_0 at which the electronic relaxation times were measured for "free" radical and vanadyl-porphyrins, correspondingly. Owing to the short repetition time, the amplitude of the FR signal is suppressed. Simulations are performed with the EasySpin package for Matlab (Stoll and Schweiger, 2006).

exponential decay of the transverse magnetization is observed with the time constants T_{2VO} within the range of 80–220 ns.

T_{2FR} magnetization curves look fancy – transverse relaxation character T_{2e} of FR deviates significantly from the exponential decay (see Figure 4.14) and are described nicely for all the investigated samples by the expression

$$I_{echo} = M_{FR} \cdot \exp\left(-\frac{2\tau}{T_{2FR}}\right) \cdot \exp\left(-m \cdot \tau^2\right), \tag{4.6}$$

where M_{FR} is a factor proportional to the concentration of FR, m is a parameter accounting for the spectral diffusion. From the analysis of relaxation times it was shown (Mamin *et al.*, 2016) that the obtained acceleration of T_{2FR} according to Equation 4.6 is caused by the spectral diffusion induced by the presence of the vanadyl porphyrin molecules in the nearest (1–3 nm) surrounding of FR. This finding can explain, for example, the fact of low polarization of FR in dynamic nuclear polarization experiments for some PDS (Alexandrov *et al.*, 2014); though the electronic relaxation times for FR are significantly longer, owing to the strong dipole–dipole FR–VO^{2+} coupling the electronic spin polarization "leaks" through the fast relaxing VO^{2+}. This finding, in our opinion, brings us one step closer to disentangling the structure of asphaltenes and the role of vanadyls in that disentangling.

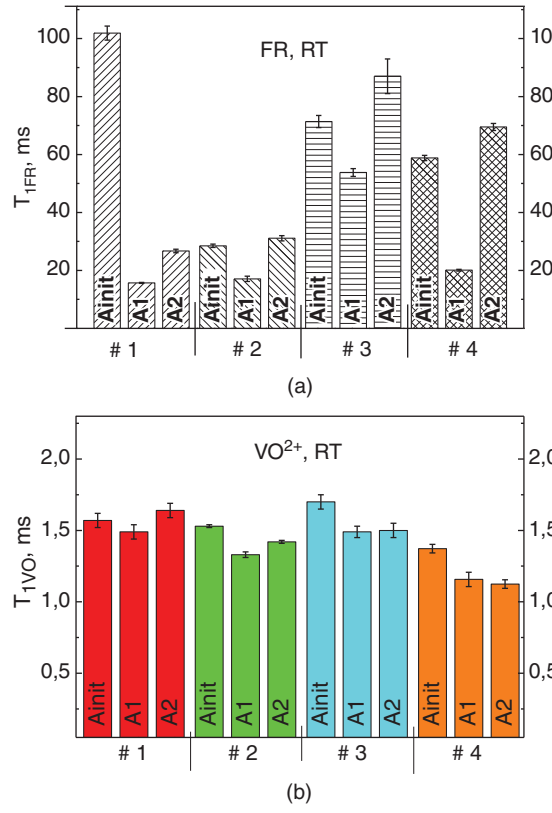

Figure 4.13 FR (a) and VO^{2+} (b) longitudinal relaxation times T_{1e} at RT for all the investigated samples.

Such "acceleration" of T_{2FR} was not reported in the literature and was not obtained by us in the X-band relaxation measurements. We connect this fact with the overlapping of FR and VO^{2+} spectra at lower frequencies (see Figure 4.4 and Section 4.2).

We have shown (Volodin *et al.*, 2013) that relaxation times, as well as intensity ratios between the FR and VO^{2+} signals (which can be determined much more accurately at high fields), can be exploited as additional parameters to characterize the origin of the crude oil and nature of the oil's PC. Indeed, concerning FR in the X-band and the lower magnetic fields, its EPR spectrum in most cases presents a single line with the linewidth of $\Delta H_{pp} = 0.4–0.7$ mT located at g-factor of 2.003 ± 0.001 (Yen, 1994, 2000; Dolomatov *et al.*, 2016). FR lineshape is neither Gaussian nor Lorentzian but a mixture of both. The non-symmetric FR spectrum, obtained in some PDS at high fields (Volodin *et al.*, 2013), could be due to the presence of two or more PCs of different origins with the close values of g-factors and/or due to the small anisotropy of g-factors.

Our experience with different PDS species proves that FR spectra in pulsed mode resemble the powder (anisotropic) spectra, they differ from each other,

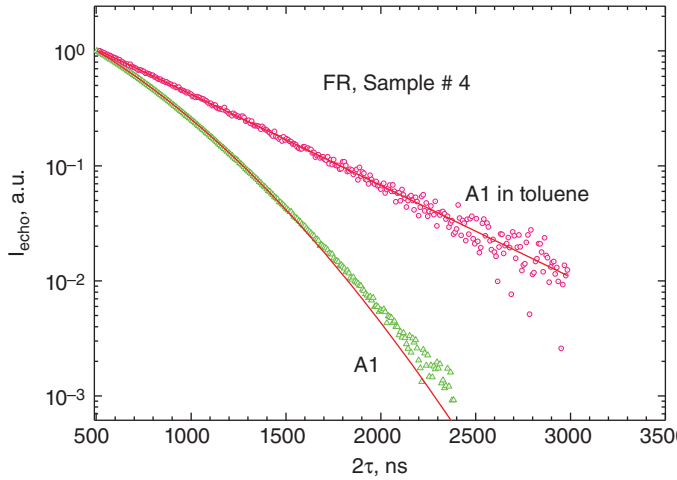

Figure 4.14 Dependencies of the primary ESE amplitude (semilog plot) on the delay τ between the two MW pulses in the pulse sequence of the sample #4 (fraction *A1*) for FR at RT. Symbols indicate the experimental data, solid lines are the results of the fits corresponding to Equation 4.6 with $m = 0$ for the fraction *A1* diluted in toluene (upper curve) and with $m = 3.6 \cdot 10^{-6}$ ns^{-2} for the undiluted fraction *A1* (lower line).

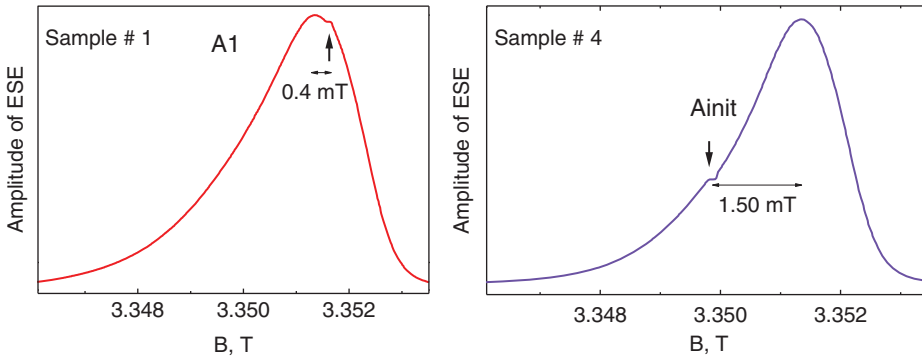

Figure 4.15 Examples of FS-ESE EPR spectra for two fractions from different samples. Splitting between the EPR features (local maxima) are shown.

and very often are split (or additional peaks appear) as Figure 4.15 shows. T_{2e} varies along the FR line. Apparently, the obtained features will be further exploited to unravel the FR nature(s).

4.4.2 ENDOR of VO^{2+} in Crude Oil Samples

There is no exclusive procedure for the isolation of porphyrin complexes from the host material (Yakubova *et al.*, 2016). Presently, one of the most promising and well-established protocols for structural characterization of

metalloporphyrins involves the application of Fourier transform ion cyclotron resonance mass spectrometry (Qian *et al.*, 2008; Zhao *et al.*, 2013, 2014; Putman *et al.*, 2014). Owing to the relatively low concentration of vanadium compounds and the very complex chemical composition of PDS, the successful identification of porphyrins requires chromatographic separation or demetalation.

The ENDOR method can complement mass spectrometry and become a part of a standard analytical toolkit. Since it does not require a special sample preparation procedure, it can be, at the very least, useful for the preliminary characterization of PDS prior to chromatographic separation.

The heavy and light crude oil samples from different oilfields (see Table 4.3) were used as received without any additional sample treatment. Figure 4.16 presents the field-swept pulsed EPR spectra of a heavy oil sample #1 detected at X- and W-bands. Figure 4.17 shows the corresponding ENDOR spectra for

Table 4.3 Samples and their physical properties at RT.

Sample	Description	Origin	Density, kg/m^3/ API gravity	Viscosity, mPa·s
#1	Heavy	Mordovo-Karmalskoye oilfield (Republic of Tatarstan, Russia)	945 / 18.2	1020
#2	(Medium) Light	The West-Siberian petroleum basin (Russia)	871 / 31	38

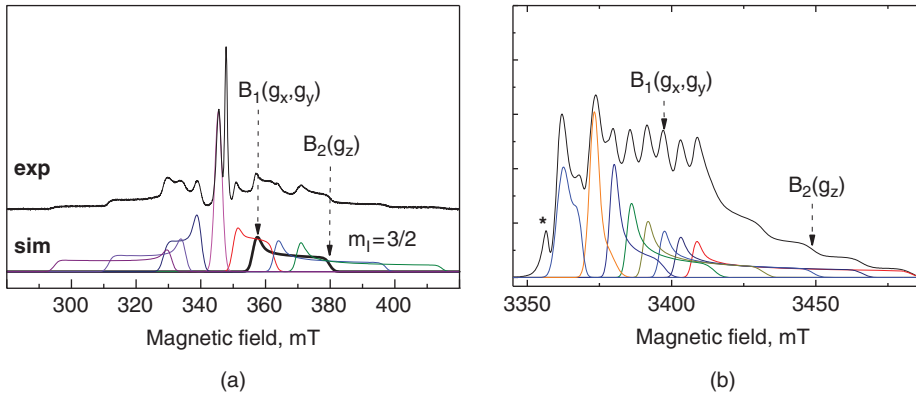

Figure 4.16 (a) X-band and (b) W-band EPR spectra at $T = 50$ K in crude oil sample #1 in pulse mode shown together with separate simulations of the different hf components due to ^{51}V nucleus. Magnetic fields B_1 and B_2 correspond to the g_Z axis parallel and perpendicular to the direction of magnetic field ($m_I = 3/2$). The signal with a *g*-factor of 2.004 related to FR is marked by an asterisk.

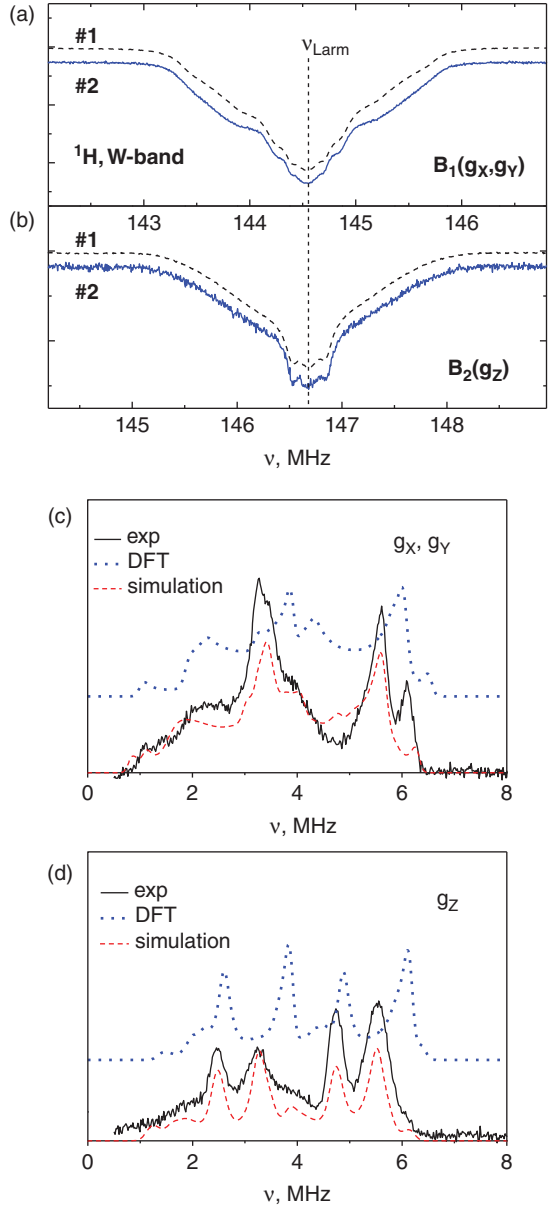

Figure 4.17 (a, b) ^{1}H Mims ENDOR spectra corresponding to different molecular orientations of vanadyl porphyrin detected in the vicinity of proton Larmor frequency at $T = 50$ K for samples #1 and #2. (c, d) ^{14}N ENDOR spectra of vanadyl porphyrins (solid curve) in X-band for crude oil samples #1, simulation (dashed curve) and calculated spectrum with parameters obtained by DFT calculations (dotted curve) at magnetic field B_1, and at magnetic field B_2. Corresponding parameters are listed in Table 4.4.

two particular values of the external magnetic field. In this work we have chosen the values that correspond mainly to the g_Z axis perpendicular (B_1) and parallel (B_2) to the direction of magnetic field for $m_I = 3/2$ transition, for the following reasons: (1) sufficient echo amplitudes to obtain reasonable signal-to-noise ratio for an appropriate amount of time; (2) absence of overlapping with the FR signal. As a result, we report observation of the ENDOR signals near the Larmor frequency of ^{1}H and ^{14}N, as displayed in Figure 4.17.

We have managed to detect for the first time pulsed ^{14}N ENDOR spectra of natural vanadyl porphyrins in the untreated heavy crude oil sample. The measured ^{14}N ENDOR spectra display the presence of both nuclear hf and electric nuclear quadrupole couplings. In order to get some prior information about the values and orientations of the corresponding interaction tensors, we have performed first-principles density functional theory (DFT) calculations (Gracheva *et al.*, 2016) on high-performance computing (HPC) clusters for complex and demanding calculations at Kazan Federal University. The results of these calculations are listed in Table 4.4 and presented in Figure 4.17. The data correspond well with those obtained from the model systems (Gracheva *et al.*, 2016).

It is known that petroleum porphyrins exist in homologous manifolds of several structural classes and can manifest great structural diversity (Gilinskaya, 2008). First of all that means different combinations of side groups. The distribution of the electric field gradient and spin density in a vanadyl porphyrin molecule can be affected by the presence of substituting

Table 4.4 Comparison between spin Hamiltonian parameters of vanadyl porphyrin complex in natural crude oil obtained from the simulation of the experimental EPR and ^{14}N ENDOR spectra and calculated by DFT method ones for VO molecule*.

	Simulation of experimental data	**DFT (VO)**
$g_X\ g_Y\ g_Z$	(1.9845 1.9845 1.9640)	(1.9867 1.9867 1.9710)
^{51}V $A_X\ A_Y\ A_Z$	|156.9 156.9 470.8|	(–157.0 –157.0 –463.9)
^{14}N $A_X\ A_Y\ A_Z$	–6.5 –7.4 –7.8	(–7.6 –7.8 –8.6)
$(\alpha\ \beta\ \gamma)_A$	(90 0 0)	(–3 10 55)
e^2Qq/h	2.2	2.24
η	0.50	0.22
$(\alpha\ \beta\ \gamma)_Q$	(30 90 180)	(40 90 –172)

*Hyperfine couplings tensor components $A_{X,Y,Z}$ and quadrupole coupling constant e^2Qq/h are in MHz. For ^{14}N coupling parameters the values are averaged over the four pyrrole nitrogen nuclei. For VO models, the variance of both hf and quadrupole coupling constants is within 0.1%. The Euler angles ($\alpha\ \beta\ \gamma$, in deg) are presented for a selected ^{14}N nucleus and specify *Z-Y-Z* rotation that transforms the molecular frame with the Z axis being perpendicular to the porphyrin plane to the frames where the hf (A) and quadrupole (Q) tensors for ^{14}N are diagonal. The coupling tensors for other three ^{14}N nuclei are consistent with C_{4v} symmetry of the molecule.

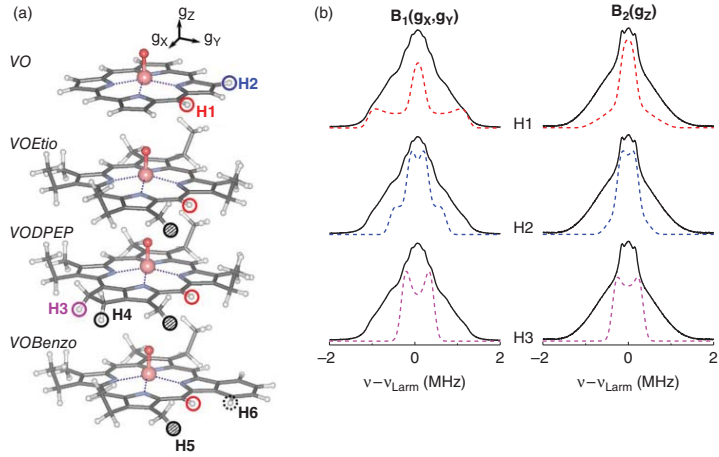

Figure 4.18 (a) Optimized chemical structures of vanadyl porphyrin models (*VO, VOEtio, VODPEP, VOBenzo*). Circles indicate the positions of the representative protons of the porphyrin skeleton (H1 and H2) and those attributed to the possible classes of side groups (H3–H6). The illustrated orientation of the *g*-tensor corresponds to the VO molecule. (b) ENDOR spectra simulated (dashed curve) for the selected protons are presented in comparison with the experimental spectra obtained for sample (solid curve).

side groups via structural perturbations of the porphyrin skeleton, thereby reducing the symmetry of pyrrole nitrogen atoms distribution around the vanadium ion. The consequent distribution of the coupling parameters can potentially increase the broadening of the spectrum, and this is probably why ^{14}N ENDOR cannot be observed in certain (or in most) oil samples. Following the discussion in Gilinskaya (2008), we propose that the possibility to detect ^{14}N ENDOR depends on the relative presence of particular forms of vanadyl porphyrins in the sample. Further experimental studies and calculations are in progress.

From the pattern of ^{1}H splittings in ENDOR spectra it is possible to infer the chemical composition of vanadyl porphyrin molecules in the studied samples (see Figure 4.18). We report observation of the reproducible pattern of hf splitting in the ^{1}H ENDOR spectra of vanadyl. We can attribute the resolved spectroscopic features to the particular positions of the protons in the porphyrin molecule. FR ENDOR studies are on the way and we hope they will shed light on the asphaltene's structure.

4.5 Conclusion

In this chapter we tried to show some capabilities of the pulsed and high-field EPR for the analysis and investigation of PDS. We hope that further research will shed light on more details of PDS dynamics and structure.

Acknowledgments

We are thankful to A. Rodionov, D. Sitdikov, A. Vakhin, A. Galukhin, Yu. Ganeeva, and T. Yusupova (Kazan, Russia) for help with the measurements and sample preparations. The main part of the research was financially supported by the Russian Ministry of Education and Science in the framework of the "5-100" Program for Kazan Federal University.

References

Adanisystems.com (2016) Adani Benchtop Analytical Instruments and Spectroscopy Official Website. Available at: http://lab.adanisystems.com.

Alexandrov, A., Archipov, R., Ivanov, A., *et al.* (2014) The low-field pulsed mode dynamic nuclear polarization in the pentavalent chromium complex and crude oils. *Appl. Magn. Reson.*, 45(10), 1275–1287.

Bruker.com (2016) Bruker Official Website. Available at: http://bruker.com.

Burlaka, A., Gafurov, M., Iskhakova, K., *et al.* (2016) Electron paramagnetic resonance in the experimental oncology: Implementation examples of the conventional approaches. *BioNanoScience*, 6(4), 431–436.

Dolomatov, M. U., Rodionov, A. A., Gafurov, M. R., *et al.* (2016) Concentration of paramagnetic centres at low-temperature thermal destruction of asphaltenes of heavy petroleum distillates. *Magn. Reson. Solids*, 18, Article No. 16101. Available at: http://mrsej.kpfu.ru/contents.html#16101.

Eaton, G., Eaton, S., Barr, D., and Weber, R. (2010) *Quantitative EPR*. Springer-Verlag, Vienna.

Evdokimov, I., Eliseev, N., and Eliseev, D. (2001) Rheological evidence of structural phase transitions in asphaltene-containing petroleum fluids. *J. Petrol. Sci. Eng.*, 30(3–4), 199–211.

Evdokimov, I., Eliseev, N., and Eliseev, D. (2004) Effect of asphaltenes on the thermal properties of emulsions encountered in oil recovery operations. *Fuel*, 83(7–8), 897–903.

Garifyanov, N. and Kozyrev, B. (1956) Paramagnetic resonance in anthracite and other carbon containing materials. *ZheTF*, 30(2), 272–276.

Gilinskaya, L. (2008) EPR spectra of V (IV) complexes and the structure of oil porphyrins. *Journ. Struct. Chem.*, 49, 245–254.

Gracheva, I, Gafurov, M., Mamin, G., *et al.* (2016) ENDOR study of nitrogen hyperfine and quadropole tensors in vanadyl porphyrins of heavy crude oils. *Magn. Reson. Solid*s, 18, Article No. 16102. Available at: http://mrsej.kpfu.ru/contents.html#16102.

Gutowsky, H., Roger Ray, B., Rutledge, R., and Unterberger, R. (1958) Carbonaceous free radicals in crude petroleum. *J. Chem. Phys.*, 28, 744–745.

Magnettech.de (2016) Magnettech Gmbh Official Website. Available at: http://magnettech.de.

Mamin, G., Gafurov, M., Yusupov, R., *et al.* (2016) Toward the asphaltene structure by electron paramagnetic resonance relaxation studies at high fields (3.4 T). *Energy Fuels*, 30 (9), 6942–6946.

Murphy, D. and Farley, R. (2006) Principles and applications of ENDOR spectroscopy for structure determination in solution and disordered matrices. *Chem. Soc. Rev.*, 35, 249–268.

O'Reilly, D. (1958) Paramagnetic resonance of vanadyl etioporphyrin I. *J. Chem. Phys.*, 29(5), 1188–1189.

Piccinato, M., Guedes, C., and Di Mauro, E. (2012) Crude oil by EPR, in: *Crude Oil Emulsions: Composition Stability and Characterization*, Abdel-Raouf, M. (ed.), Rijeka, Croatia: InTech, 147–168.

Putman, J., Rowland, S., Corilo, Y., and McKenna, A. (2014) Chromatographic enrichment and subsequent separation of nickel and vanadyl porphyrins from natural seeps and molecular characterization by positive electrospray ionization FT-ICR mass spectrometry. *Analytical Chemistry*, 86(21), 10708–10715.

Qian, K., Mennito, A., Edwards, K., and Ferrughelli, D. (2008) Observation of vanadyl porphyrins and sulfur-containing vanadyl porphyrins in a petroleum asphaltene by atmospheric pressure photonionization Fourier transform ion cyclotron resonance mass spectrometry. *Rapid Communications in Mass Spectrometry*, 22(14), pp 2153–2160.

Qin, P. and Warncke, K. (2015a) Electron paramagnetic resonance investigations of biological systems by using spin labels, spin probes, and intrinsic metal ions: Part A. *Methods in Enzymology*, 563, 2–684.

Qin, P. and Warncke, K. (2015b) Electron paramagnetic resonance investigations of biological systems by using spin labels, spin probes, and intrinsic metal ions: Part B. *Methods in Enzymology*, 564, 2–613.

Ramachandran, V., van Tol, J., McKenna, A., *et al.* (2015) High field electron paramagnetic resonance characterization of electronic and structural environments for paramagnetic metal ions and organic free radicals in Deepwater Horizon oil spill tar balls. *Anal. Chem.*, 87(4), 2306–2313.

Schweiger, A. and Jeschke, G. (2001) *Principles of Pulse Electron Paramagnetic Resonance*. Oxford University Press, Oxford.

Stoll, S. and Schweiger, A. (2006) EasySpin, a comprehensive software package for spectral simulation and analysis in EPR. *J. Magn. Reson.*, 178, 42–55.

Syunyaev, Z. (1980) Concentration of complex structural units in disperse petroleum systems and methods for regulation of this concentration. *Chemistry and Technology of Fuels and Oils*, 16(7), 484–489.

Tayeb Ben, K., Delpoux, O., Barbier, J., *et al.* (2015) Applications of pulsed electron paramagnetic resonance spectroscopy to the identification of vanadyl complexes in asphaltene molecules: Part 1: Influence of the origin of the feed. *Energy Fuels*, 29(7), 4608–4615.

Trukhan, S., Yudanov, V., Gabrienko, A., *et al.* (2014) In situ electron spin resonance study of molecular dynamics of asphaltenes at elevated temperature and pressure. *Energy Fuels*, 28(10), 6315–6321.

Volodin, M., Mamin, G., Izotov, V., and Orlinskii, S. B. (2013) High-frequency EPR study of crude oils. *J. Phys. Conf. Ser.*, 478, Art. No. 012003.

Wang, W., Ma, Y., Li, S., *et al.* (2016) Effect of temperature on the EPR properties of oil shale pyrolysates. *Energy Fuels*, 30(2), 830–834.

Yakubova, M., Milordova, D., Yakubova, S., *et al.* (2016) Features of the composition of vanadyl porphyrins in the crude extract of asphaltenes of heavy oil with high vanadium content. *Petroleum Science and Technology*, 34(2), 177–183.

Yaviar.ru (2016) Yaviar, Ltd. Official Website. Available at: http://yaviar.ru/produktsiya/spektrometry.

Yavkin, B., Mukhambetov, I., Lamberov, A., and Orlinskii, S. B. (2014) Electron paramagnetic resonance and electron nuclear double resonance study of the paramagnetic complexes of anthraquinone on the surface of γ-Al2O3. *Journal of Physical Chemistry C*, 118(27), 14998–15003.

Yen, T. and Chilingarian, G. (1994) *Asphaltenes and Asphalts: 1: Developments in petroleum science: 40A*, Elsevier, New York.

Yen, T. and Chilingarian, G. (2000) *Asphaltenes and Asphalts: 2: Developments in petroleum science: 40 B*, Elsevier, New York.

Zavoisky, E. (1945) Paramagnetic relaxation of liquid solutions for perpendicular fields. *Journal of Physics (Academy of Sciences of the USSR)*, 9(3), 211–216.

Zhao, X., Liu, Y., Xu, C., *et al.* (2013) Separation and characterization of vanadyl porphyrins in Venezuela Orinoco heavy crude oil. *Energy Fuels*, 27(6), 2874–2882.

Zhao, X., Shi, Q., Gray, M., and Xu, C. (2014) New vanadium compounds in Venezuela heavy crude oil detected by positive-ion electrospray ionization Fourier transform ion cyclotron resonance mass spectrometry. *Scientific Reports*, 4. Art. No 5373.